Two-dimensional map for impact oscillator with drift

Ekaterina Pavlovskaia* and Marian Wiercigroch†
Centre for Applied Dynamics Research, Department of Engineering, King's College, Aberdeen University, Aberdeen AB24 3UE, United Kingdom

Celso Grebogi‡
Instituto de Física, Universidade de São Paulo, Caixa Postal 66318, 05315-970 São Paulo, São Paulo, Brazil
(Received 2 April 2004; published 8 September 2004)

An impact oscillator with drift is considered. The model accounts for viscoelastic impacts and is capable of mimicking the dynamics of progressive motion, which is important in many applications. To simplify the analysis of this system, a transformation decoupling the original coordinates is introduced. As a result, the bounded oscillations are separated from the drift motion. To study the bounded dynamics, a two-dimensional analytical map is developed and analyzed. In general, the dynamic state of the system is fully described by four variables: time τ, relative displacement p and velocity y of the mass, and relative displacement q of the slider top. However, this number can be reduced to two if the beginning of the progression phase is being monitored. The lower and upper bounds of the map domain are approximated. A graphical method of iteration of the two-dimensional map, similar to the cobweb method used in the one-dimensional case, is proposed. The results of numerical iterations of this two-dimensional map are presented, and a comparison is given between bifurcation diagrams calculated for this map and for the original system of differential equations.

DOI: 10.1103/PhysRevE.70.036201 PACS number(s): 05.45.−a

I. INTRODUCTION

The dynamics of impacting systems that drift during operation is of considerable importance in practical applications. A wide range of models have been applied to analyze engineering systems operating within bounded dynamic responses. For example, in heat exchanger tubes [1], thin-wall milling [2], ultrasonic drilling of hard materials [3], and vibroimpact ground moling systems [4], impacting models have proved to be useful. The fundamental dynamic behavior of impact oscillators has been much studied in the past (e.g., [5–11]) and shows great complexity and sensitivity to the system parameters and the initial conditions. In most cases it is assumed that the impacting system or its elements oscillate about their equilibrium positions. Only recently has a combination of bounded oscillations and drifting motion started to be considered [12–16]. The coordinate transformation proposed in [16] significantly simplifies the analysis of an impact oscillator with drift as it allows one to apply standard nonlinear dynamic techniques, and thus study the bounded oscillations separately from the progressive motion and reconstruct the drift of the system afterward. In the current study, an implicitly defined map of reduced dimension is developed, similar to those introduced in [17–22].

The system considered in this work belongs to a class of piecewise smooth systems, whose dynamics are known to exhibit complex bifurcation scenarios and chaos. These systems can undergo all types of bifurcations that smooth ones do, but apart from them there is whole class of bifurcations that are unique to piecewise smooth systems such as grazing [10,23,24], chattering [25], and sliding [26]. A good deal of work has been done to study these special bifurcations using normal form maps which were derived based on the system's original differential equations (see for example, [26–28]). The general bifurcation scenarios in explicitly defined two-dimensional piecewise smooth maps were also considered in [11,29]. However, it is difficult to apply the developed bifurcation theory to the map introduced in the current study as it is defined implicitly. It should be noted also that, although the impact oscillator [16] can certainly undergo grazing bifurcations, they are beyond the scope of the present study.

The paper is organized as follows. In the next section, the considered impact oscillator is described and equations for each phase of motion are given. Then the two-dimensional map is defined on a finite domain, whose boundaries are analytically determined. The numerical results are presented and discussed in Sec. IV, and finally the conclusions are drawn.

II. IMPACT OSCILLATOR WITH DRIFT

We consider the simple two-degrees-of-freedom oscillator shown in Fig. 1. A mass m is driven by an external force f containing static b and dynamic $a\cos(\omega\tau+\varphi)$ components. The weightless slider has a linear viscoelastic pair of stiffness k and damping c. The system is nondimensionalized, where τ, 2ξ, f, b, a, and ω are the nondimensional time, damping coefficient, force, static component, and amplitude and frequency of the dynamic component, respectively. As has been reported in [14], the slider drifts in stick-slip phases where the relative oscillations between the mass and the slider are bounded and range from periodic to chaotic. Similarly to the stick-slip phenomena reported in [30,31], the progressive motion of the mass occurs when the force acting on the slider exceeds the threshold of the dry friction force d.

*Electronic address: E.Pavlovskaia@eng.abdn.ac.uk
†Electronic address: M.Wiercigroch@eng.abdn.ac.uk
‡Electronic address: grebogi@if.usp.br

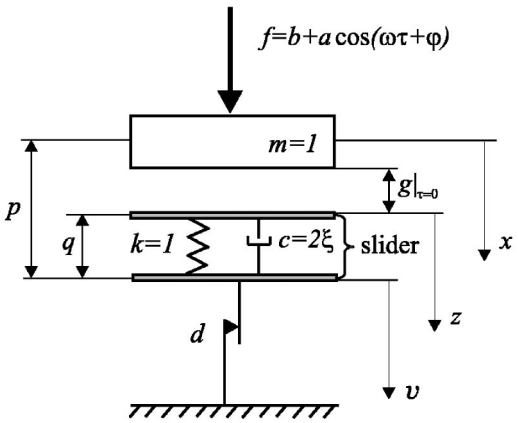

FIG. 1. Physical model of impact system with drift.

The variables x,z,v represent the absolute displacements of the mass, slider top, and slider bottom, respectively. It is assumed that the model operates in the horizontal plane, or the gravitational force is appropriately compensated. At the initial instant $\tau=0$, there is a gap between the mass and the slider top, indicated by g. The difference $(z+g)-x$ allows monitoring of the gap size. To simplify the subsequent analysis, the dimensionless friction threshold force d is set to 1, and we also set $\varphi=\pi/2$ and initial gap $g=0.02$.

The system under consideration can operate in one of the following modes: *no contact*, *contact without progression*, and *contact with progression*. A detailed description of these modes, the dimensional form of the equations of motion, and details of the nondimensionalization procedure can be found in [14]. As reported in [16], by introducing the system of coordinates (p,q,v), defined in terms of (x,z,v), as

$$p = x - v,$$

$$q = z - v, \tag{1}$$

it is possible to separate the oscillatory motion of the system from the drift. In fact, in this coordinate system, p and q are the displacements of the mass and the slider top, relative to the current position of the slider bottom v. In this study, we consider bounded oscillations and attempt to reconstruct the progressive motion.

For the purpose of clarity, a brief review summarizing how all particular phases of the dynamic responses are defined is given next. The corresponding nondimensionalized equations of motion consist of a system of four first-order differential equations.

No contact. If the distance between the mass and the slider top is greater than zero, $q+g-p>0$, then the mass and the slider top move separately. The equations of motion are the following:

$$p' = y,$$

$$y' = a\cos(\omega\tau+\varphi)+b \quad \text{for} \quad p < q+g,$$

$$q' = -\frac{1}{2\xi}q,$$

$$v' = 0. \tag{2}$$

Contact without progression. This mode occurs when the distance between the mass and the slider top is equal to zero, i.e., $q+g-p=0$, and the force acting on the mass from the slider is greater than zero but smaller than the threshold of the dry friction force. The equations of motion are in this case

$$p' = y,$$

$$y' = -2\xi y - q + a\cos(\omega\tau+\varphi)+b \quad \text{for} \quad p = q+g$$
$$\text{and} \quad 0 < 2\xi y + q < d,$$

$$q' = y,$$

$$v' = 0. \tag{3}$$

Contact with progression. When the distance between the mass and the slider top is equal to zero, $q+g-p=0$, and the force acting on the mass is greater than the threshold of the dry friction force, then the mass and the top and the bottom of the slider move together, and progression takes place. We have the following equations of motion:

$$p' = -\frac{1}{2\xi}(q-d),$$

$$y' = a\cos(\omega\tau+\varphi)+b-d \quad \text{for} \quad p = q+g \quad \text{and} \quad 2\xi y + q \geqslant d,$$

$$q' = -\frac{1}{2\xi}(q-d),$$

$$v' = y + \frac{1}{2\xi}(q-d). \tag{4}$$

The equations of motion are linear for each phase; therefore the global solution can be constructed by joining the local solutions at the points of discontinuities. The set of initial values $(\tau_0;p_0,y_0,q_0)$ defines in which phase the system will operate. If $p_0<q_0+g$, it is the *no contact* phase. For $p_0=q_0+g$, it will be the *contact without progression* phase if $0<2\xi y_0+q_0<d$ or the *contact with progression* phase if $2\xi y_0+q_0\geqslant d$. The solutions for all specified phases are given in Appendix A. When the conditions corresponding to the current phase fail, the next phase begins, and the final displacements and velocities for the preceding phase define the initial conditions for the next one. All details of the semianalytical method allowing calculation of the responses of the system using this method are given in [15].

As was mentioned before, the progression $v(\tau)$ can be calculated separately if the dynamics of the bounded system (p,y,q) is known (i.e., the sequence of the phases and the initial conditions for them). Since during the *no contact* and the *contact without progression* phases the progression does not change its value,

$$v(\tau) = v_0. \tag{5}$$

For the *contact with progression* phase, $v(\tau)$ can be expressed as

$$v(\tau) = v_0 + p_0 - g - d - (p_0 - g - d)\exp\left(-\frac{\tau - \tau_0}{2\xi}\right) + y_0(\tau - \tau_0) + \frac{b-d}{2}(\tau - \tau_0)^2 - \frac{a}{\omega^2}[\cos(\omega\tau + \varphi) - \cos(\omega\tau_0 + \varphi) + \omega(\tau - \tau_0)\sin(\omega\tau_0 + \varphi)]. \quad (6)$$

III. TWO-DIMENSIONAL MAP

To study the dynamics of the system under investigation, a two-dimensional (2D) map is derived next and its dynamics is analyzed. In general, the dynamic state of the system is fully described by four variables: time τ, relative displacement p and velocity y of the mass, and relative displacement of the slider top q. This means that if a set of initial conditions $(\tau_0; p_0, y_0, q_0)$ is given, the subsequent behavior of the system can be calculated. However, this number of dynamical variables can be reduced to two if the beginning of the progression phase is to be monitored. Let us assume that the progression phase starts at $\tau = \tau_*$ and at this moment $p = p_*, y = y_*$, and $q = q_*$. Then we note that the beginning of the progression phase is defined as the moment when the force acting on the slider has reached the critical value, i.e., the following condition is satisfied:

$$2\xi y_* + q_* = d,$$

which means that, at this moment, y_* and q_* are linearly dependent as

$$q_* = d - 2\xi y_*. \quad (7)$$

Also during both types of contact phase (with and without progression) the relative displacements of the mass and the slider top remain linearly related as

$$p_* = q_* + g,$$

and taking into account relationship (7), we have

$$p_* = d - 2\xi y_* + g. \quad (8)$$

Thus, only the two independent variables y_* and τ_* are needed to fully describe the dynamic state of the system in the beginning of the progression phase. Instead of the time τ_* one can use the angular displacement

$$\psi_* = \varphi + \omega\tau_*. \quad (9)$$

Let us assume that the velocity y_* and angular displacement ψ_* for the nth occurrence of the beginning of the progression phase are described simply as y_n and ψ_n. Consequently the pair (y_n, ψ_n) can be used to construct a 2D map

$$y_{n+1} = f_1(y_n, \psi_n),$$

$$\psi_{n+1} = f_2(y_n, \psi_n), \quad (10)$$

which is the main motivation for this study.

The mapping (10) contains different phases whose number and sequence are not known. First of all the system goes through the progression phase, whose duration $\eta(y_n, \psi_n)$ can be calculated from

$$2\xi y^{III}(\eta) + q^{III}(\eta) - d = 0, \quad (11)$$

where the functions $y^{III}(\tau)$ and $q^{III}(\tau)$ are given by Eq. (A5) for $y_0 = y_n, \tau_0 = (\psi_n - \varphi)/\omega$, and $q_0 = d - 2\xi y_n$.

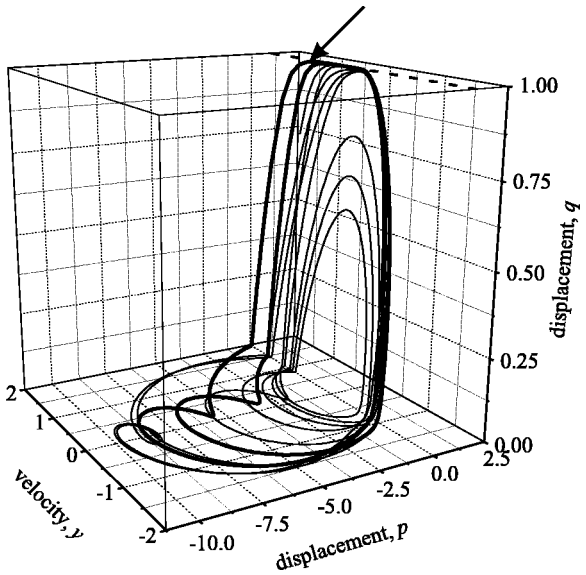

FIG. 2. Trajectory of the system for period-2 motion (thick line, $b = 0.12$) and chaotic motion (thin line, $b = 0.1$) for $a = 0.3, \xi = 0.01, \omega = 0.1$. The trajectory coincides with the dashed line during the contact with progression phase, and an arrow indicates the beginning of this phase, which is used in constructing the 2D map.

Next the system has the *contact without progression* phase. Here there are two possible options as at the end of this phase the system can be either at the beginning of the *contact with progression* phase or at the beginning of the *no contact* phase. In the first case the duration $\sigma^I(y_n, \psi_n)$ of this *contact without progression* phase can be determined from

$$2\xi y^{II}(\sigma^I) + q^{II}(\sigma^I) - d = 0. \quad (12)$$

In the second case, the duration $\sigma^{II}(y_n, \psi_n)$ is also described implicitly by

$$2\xi y^{II}(\sigma^{II}) + q^{II}(\sigma^{II}) = 0. \quad (13)$$

In both cases the functions $y^{II}(\tau)$ and $q^{II}(\tau)$ are given by Eq. (A2), substituting $\tau_0 = (\psi_n - \varphi)/\omega + \eta(y_n, \psi_n)$, and p_0, y_0, and q_0 by the initial values of $p^{III}(\eta), y^{III}(\eta)$, and $q^{III}(\eta)$ for this *contact without progression* phase.

For the first case we have already obtained (y_{n+1}, ψ_{n+1}) as a function of (y_n, ψ_n):

$$\psi_{n+1} = \psi_n + \omega(\eta(y_n, \psi_n) + \sigma(y_n, \psi_n)),$$

$$y_{n+1} = y^{II}(\sigma^{II}(y_n, \psi_n)). \quad (14)$$

For the second case calculations should be continued until the system reaches the beginning of the *contact with progression* phase. After the *contact without progression* phase the system goes through the *no contact* phase and then again through the *contact without progression* phase. At the end of

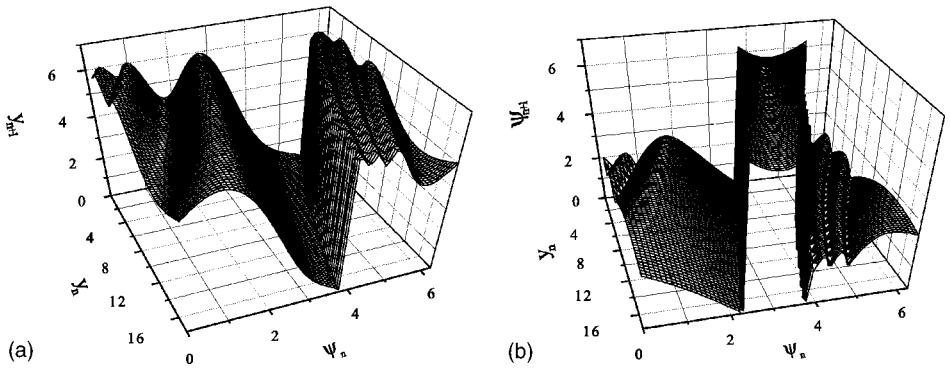

FIG. 3. 2D maps $y_{n+1}=f_1(y_n,\psi_n)$ and $\psi_{n+1}=f_2(y_n,\psi_n)$ calculated for $a=0.3, b=0.1, \xi=0.01, \omega=0.1$.

this *contact without progression* two scenarios are possible as the system can reach either the *no contact* phase or the *contact with progression* phase. In the latter case the next values (y_{n+1},ψ_{n+1}) are obtained, whereas otherwise the calculations should be continued.

Even for the simplest case when (y_{n+1},ψ_{n+1}) as a function of (y_n,ψ_n) is given by Eqs. (14), the relationships between the current and subsequent positions of the system at the beginning of the progression phase are implicit, so we can introduce the general implicit 2D map

$$f_y(y_n,\psi_n,y_{n+1},\psi_{n+1})=0,$$

$$f_\psi(y_n,\psi_n,y_{n+1},\psi_{n+1})=0. \tag{15}$$

The map (15) can be determined as described above by using Eqs. (A1)–(A5), which avoids direct numerical integration and reduces the problem to solving a set of nonlinear algebraic equations.

To make the understanding of the physical meaning of the proposed map (15) easier, let us consider a trajectory in three dimensions. In Fig. 2, two time histories of period-2 and of chaotic motion are marked by thick and thin lines, respectively. When the system is in the *no contact* phase, the trajectory is in the vicinity of the $q=0$ plane. Once the mass hits the slider, the trajectory goes out of the $q=0$ plane, and during most of the *contact with progression* phase it is on the line $p\approx 1+g, q\approx 1$, which is marked by a dashed line. The map (15) allows prediction of only the beginning of the *contact with progression* phase, which is indicated by an arrow, and does not monitor entirely the dynamics between the two subsequent *contact with progression* phases. Also, it should be noted that the time between these two subsequent phases is not known *a priori*, and the chaotic motion given by the thin line in Fig. 2 demonstrates that there could be quite a few *no contact* and *contact without progression* phases before the next progression occurs.

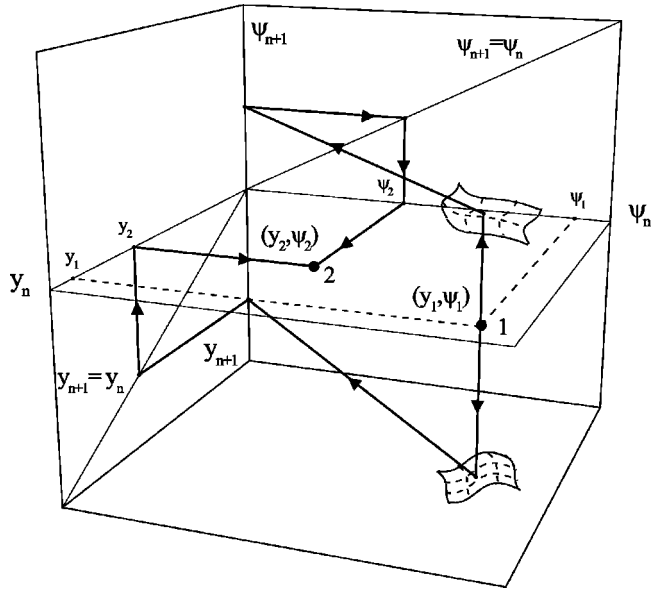

FIG. 4. Cobweb for a 2D mapping.

Graphical representations of the map (15) are shown in Fig. 3, computed for $y\in(0,17.5)$ and $\psi\in(0,2\pi)$. As the latter domain is perfectly justifiable, an estimation of the maximum velocity is far from straightforward and will be explained below.

In order to effectively iterate the 2D map (15), a good estimation of the domain of ψ_n and y_n should be determined. The periodicity of the external force allows us to use the angular displacement ψ_n instead of the time τ_n and thus $\psi_n\in(0,2\pi)$. During the progression phase the velocity of the mass y_n is greater than zero, so $y_n>0$, and, as shown in Appendix B, the maximum velocity y_n^{max} is limited. The estimation of the maximum value of y_n can be given as

$$y_n^{max}<\omega K_1+\sqrt{(b+K_1)^2+\frac{1}{1-\xi^2}(K_3-\xi b+K_1\sqrt{\xi^2+\omega^2})^2}, \tag{16}$$

where

$$K_1=\frac{a}{\sqrt{(1-\omega^2)^2+4\xi^2\omega^2}}, \tag{17}$$

$$K_2=\sqrt{(1-b+K_1)^2+\frac{1}{1-\xi^2}[\xi(1-b)+K_1\sqrt{\xi^2+\omega^2}]^2},$$

$$K_3=\frac{3a}{\omega}+\omega K_1+K_2+\sqrt{2b\left(K_1+K_2-b+\frac{2a}{\omega^2}\right)+\left(\frac{a}{\omega}+\omega K_1+K_2\right)^2}. \tag{18}$$

It should be noted here that although the value given in the

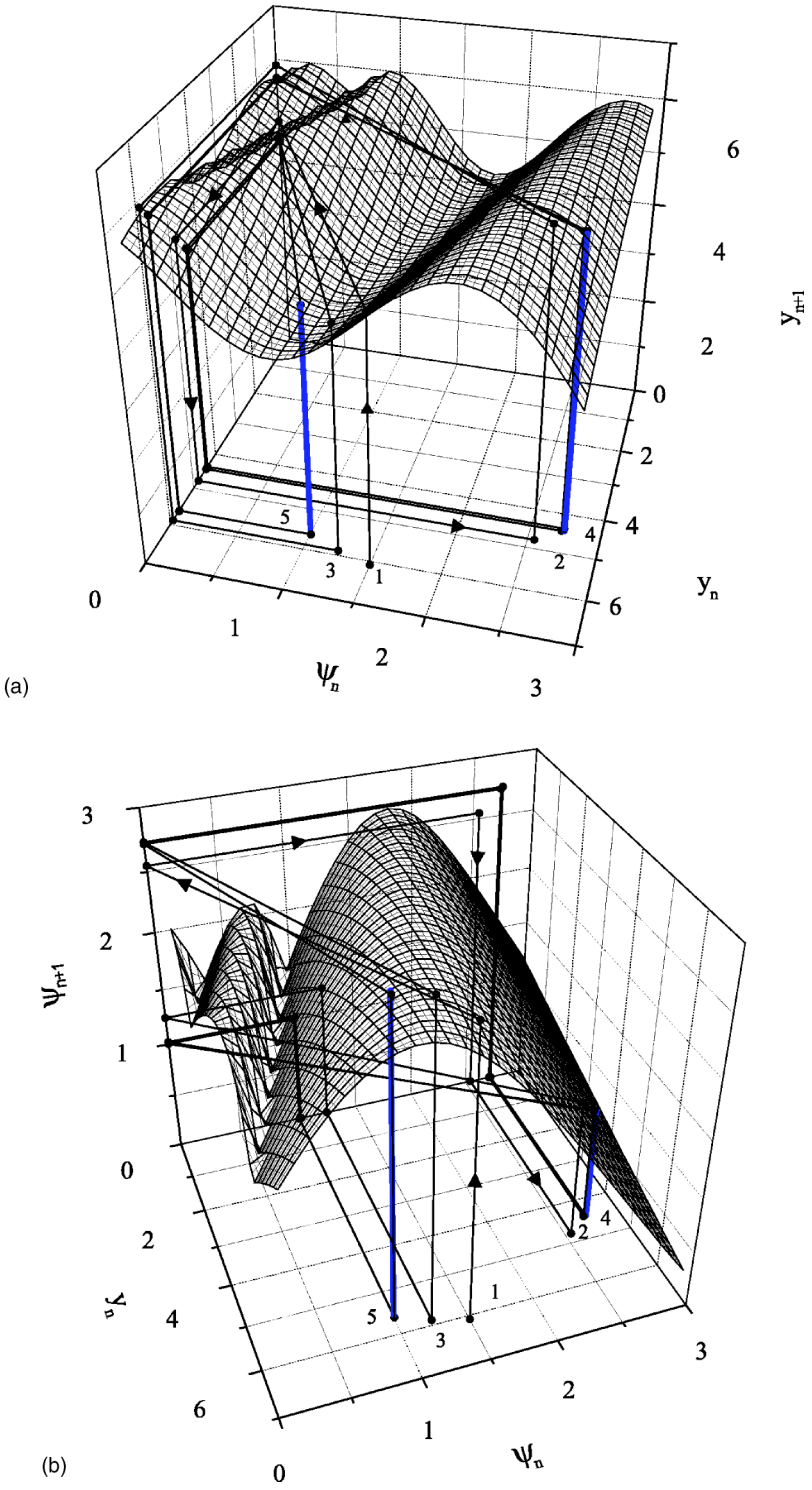

FIG. 5. Iterations of 2D maps $y_{n+1}=f_1(y_n,\psi_n)$ and $\psi_{n+1}=f_2(y_n,\psi_n)$ calculated for $a=0.3, b=0.1, \xi=0.01, \omega=0.1$.

inequality (16) will never be reached (see Appendix B), it gives the upper band for y_n.

Now the constructed 2D map can also be used to study the system stability and, for that, a method similar to the cobweb method in 1D is developed, which is shown schematically in Fig. 4. The iteration of the map starts from the point (y_1,ψ_1) on the (y_n,ψ_n) plane. In this figure, the upper half space is used to represent the surface $\psi_{n+1}=f_2(y_n,\psi_n)$ and the lower half space represents the surface $y_{n+1}=f_1(y_n,\psi_n)$.

The intersections of the vertical line positioned at (y_1,ψ_1) with the surfaces y_{n+1} and ψ_{n+1} determine y_2 and ψ_2. To iterate the map, these values need to be brought onto the (y_n,ψ_n) plane again, which is done by reflecting the point ψ_2 about the line $\psi_{n+1}=\psi_n$ in the (ψ_n,ψ_{n+1}) plane; the point y_2 is reflected relative to the line $y_{n+1}=y_n$ in the (y_n,y_{n+1}) plane.

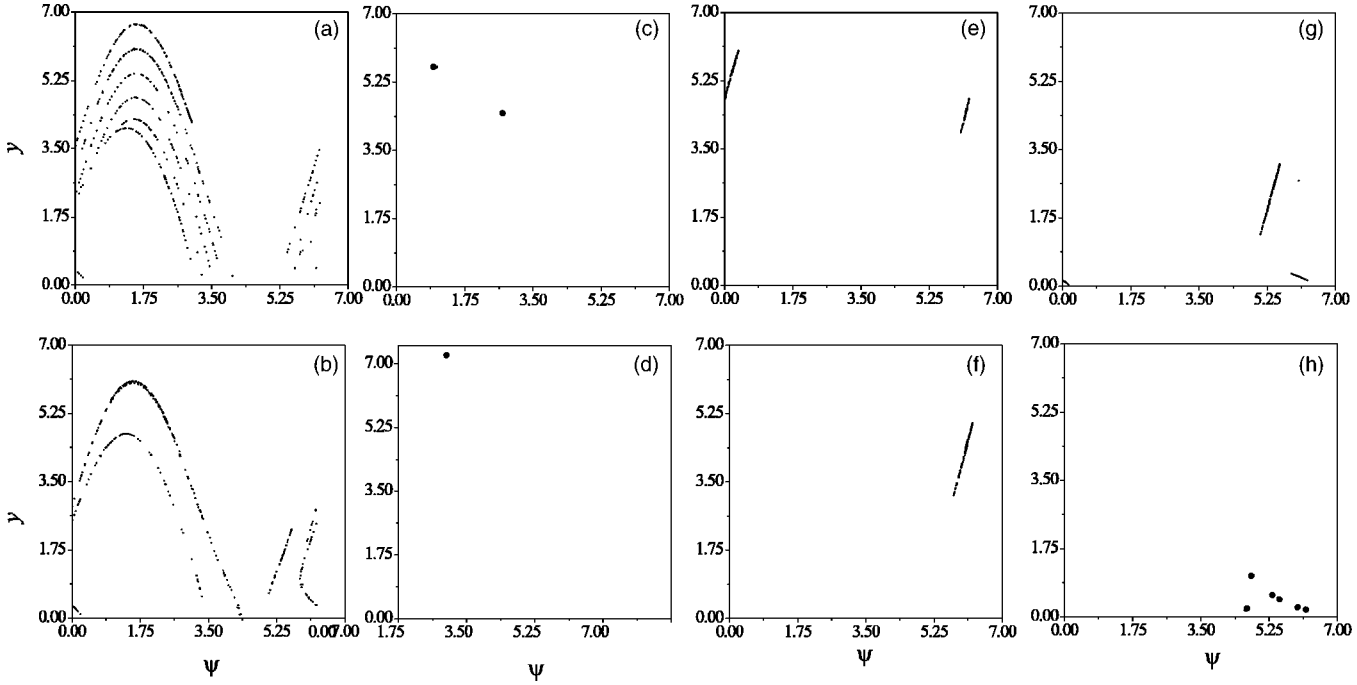

FIG. 6. 2D maps computed for $a=0.3, \xi=0.01, \omega=0.1$, and (a) $b=0.02$, (b) $b=0.05$, (c) $b=0.1$, (d) $b=0.15$, (e) $b=0.18$, (f) $b=0.2$, (g) $b=0.24$, (h) $b=0.29$.

So the next point (y_2, ψ_2) on the (y_n, ψ_n) plane is obtained, and the iteration procedure can be restarted. If for the given set of parameters the system has a stable periodic solution, a fixed point on the (y_n, ψ_n) plane will be found.

Iteration of the 2D map shown in Fig. 3 is demonstrated in Fig. 5. To make this picture clearer, only the last part of the iteration process converging to the period-2 solution is shown. The iteration starts from points 1 on both graphs. Following the thin lines with arrows, according to the method described above, one can obtain the next points on (y_n, ψ_n) plane. Here points 4 and 5 are already very close to the period-2 orbit whose intersections with the surfaces y_{n+1} and ψ_{n+1} are marked by thick vertical lines.

IV. PERIODIC AND CHAOTIC ORBITS

Some results from iterations of the 2D map are shown on the (y_n, ψ_n) plane in Fig. 6. As can be seen, the motion of the system varies from chaotic to different periodic orbits. In contrast to the classical Poincaré map where the trajectory is sampled once per period of the external excitation, for this map, the points are taken at the beginning of the *contact with progression* phase. As a result, the duration and shape of the periodic orbit are not known *a priori*. For example, period-1 motion, shown in Fig. 6(d), represents periodic response for which the *contact with progression* phase occurs once, and its period is $2\pi/\omega$, whereas for period-6 motion, shown in Fig. 6(h), the *contact with progression* phase occurs six times, and its period is $4\pi/\omega$. In Fig. 7, two different period-2 motions are shown using 2D maps [Figs. 7(a) and 7(b)] and phase portraits [Figs. 7(c) and 7(d)]. These motions not only differ in the shape of the orbits, but they also have different periods, equal to $4\pi/\omega$ and $2\pi/\omega$ for Figs. 7(a) and 7(c) and Figs. 7(b) and 7(d), respectively.

A comparison of bifurcation diagrams calculated for the proposed 2D map and for the original set of piecewise linear ordinary differential equations, Eqs. (2)–(4), is given in Fig. 8. The diagram presented in Fig. 8(a) is constructed by taking 300 points in the beginning of the progression phase, after eliminating the transient processes (first 100 points of the map iteration), while the diagram presented in Fig. 8(b) is constructed by taking 300 points, once per period of external excitation, also after the transient process has died down (which is assumed to last for 100 periods). As can clearly be seen from this figure for most values of the static force b, both diagrams indicate the same type of regime. However, there are several values (for example, $b=0.27$ marked by the dashed line) where the period-2 orbit shown in Fig. 8(a) appears as period-1 orbit in Fig. 8(b). This is because the duration of one iteration of the 2D map is not constant, and for $b=0.27$ during one period of external excitation the progression phase occurs twice.

As was mentioned earlier, the proposed 2D map contains sufficient information to recalculate all characteristics of the system dynamics, including the progression. For a given point (ψ_*, y_*) of the (ψ_n, y_n) plane, the duration T of the *contact with progression* phase is found by solving the nonlinear algebraic equation $2\xi y^{III}(\tau_*+T)+q^{III}(\tau_*+T)=d$, where $\tau_*=(\psi_*-\varphi)/\omega$. After substituting the functions $y^{III}(\tau)$ and $q^{III}(\tau)$ from Eqs. (A5) and q_* from Eq. (7) one obtains

$$y_* + (b-1)T + \frac{a}{\omega}[\sin(\omega T + \psi_*) - \sin(\psi_*)] - \exp\left(-\frac{T}{2\xi}\right) = 0. \tag{19}$$

Once Eq. (19) is solved, by substituting p_* from Eq. (8) into Eq. (6), the progression v_* during this phase can be expressed as

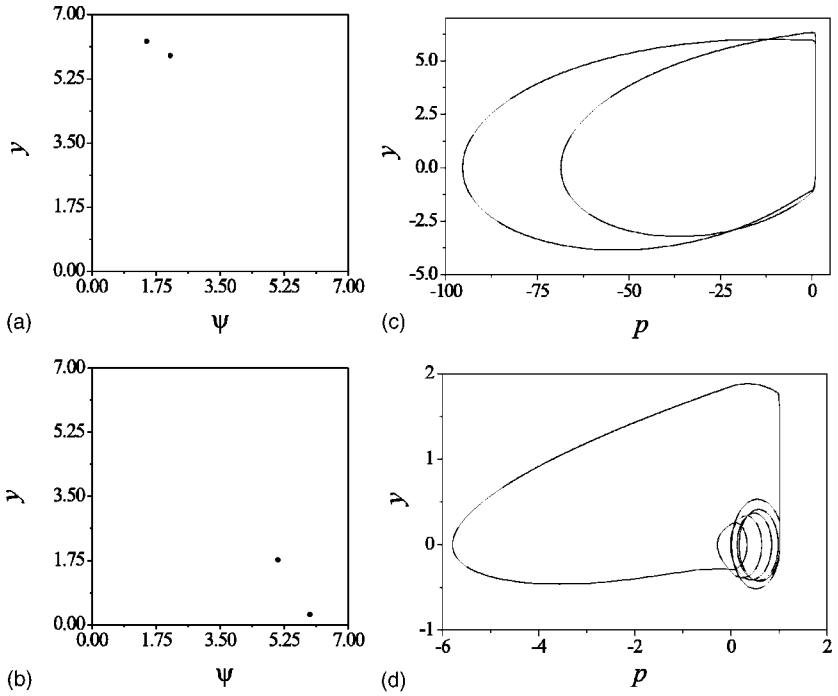

FIG. 7. (a),(b) 2D maps and (c),(d) phase portraits computed for $a=0.3, \xi=0.01, \omega=0.1$, and (a),(c) $b=0.11$ and (b),(d) $b=0.27$.

$$v_* = -2\xi y_* + 2\xi y_* \exp\left(-\frac{T}{2\xi}\right) + y_* T + \frac{b-1}{2}T^2 - \frac{a}{\omega^2}[\cos(\omega T + \psi_*) - \cos(\psi_*) + \omega T \sin(\psi_*)]. \quad (20)$$

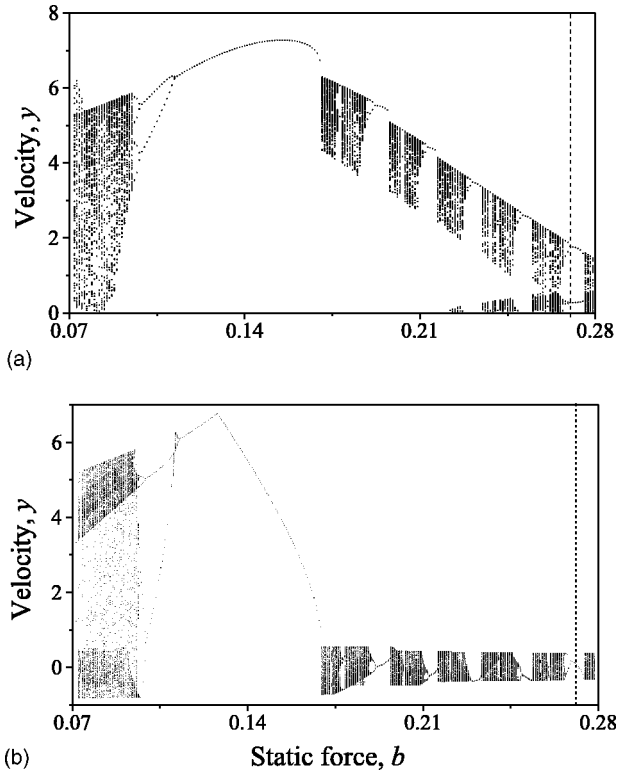

FIG. 8. Bifurcation diagrams computed for $a=0.3, \xi=0.01, \omega=0.1$ for (a) the developed 2D map and (b) the original set of piecewise linear ordinary differential equations Eqs. (2)–(4).

The period-2 motion shown in Figs. 7(a) and 7(c) for $b=0.11$ has two *contact with progression* phases. The first of them is described by $\psi_{*1}=2.142\,21$, and $y_{*1}=5.884\,28$. According to Eq. (19), it lasts for a time $T_1=5.300\,76$, and, according to Eq. (20), it has the progression $v_{*1}=15.7256$. The second *contact with progression* phase is described by $\psi_{*2}=1.501\,47$, and $y_{*2}=6.279\,03$, it lasts for a time $T_2=6.509\,02$, and has the progression $v_{*2}=20.9695$. Thus the total progression per period for this motion is $v_{*1}+v_{*2}=36.6951$. For the period-2 motion shown in Figs. 7(b) and 7(d) for $b=0.27$, we have $\psi_{*1}=5.9506, y_{*1}=0.272\,31$, $T_1=0.613\,85$, $v_{*1}=0.077\,960\,2$ and $\psi_{*2}=5.075\,41, y_{*2}=1.775\,33$, $T_2=3.046\,63$, $v_{*2}=2.607\,51$, and the total progression per period is 3.660 48. Thus, taking into account the difference in the periods for these regimes, we can deduce that during the same time the progression for $b=0.11$ will be approximately five times larger than for $b=0.27$.

Equations (19) and (20) allow us to calculate the duration of the *contact with progression* phase and the progression as functions of initial angular displacement ψ_* and velocity y_* and, consequently, to construct T and v_* as functions of (y_*, ψ_*). The surfaces $T(\psi_*, y_*)$ and $v(\psi_*, y_*)$ presented in Fig. 9 clearly show the level of progression for the given set of system parameters and might be useful from the application point of view, in particular to develop effective control strategies.

V. CONCLUSIONS

In this paper, an impact oscillator with a drift was considered. To study the bounded dynamics of the system, a two-

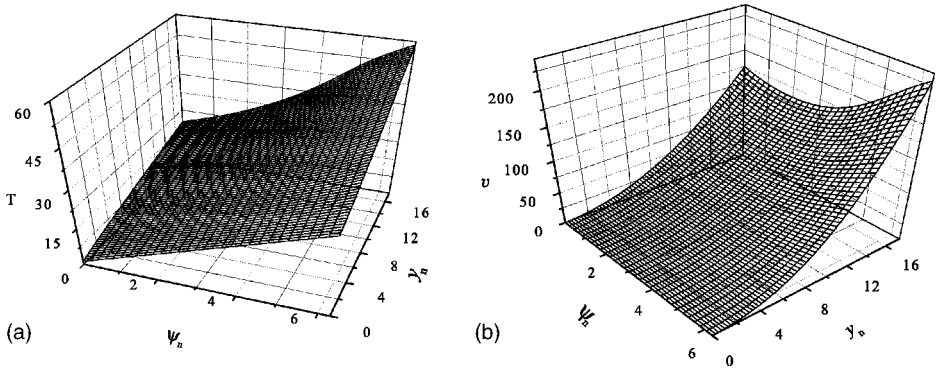

FIG. 9. (a) Duration of *contact with progression* phase, T, and (b) achieved progression, v, as function of ψ_n and y_n, calculated for $a=0.3, \xi=0.01, \omega=0.1$, and $b=0.15$.

dimensional analytical map was developed and analyzed. In general, the dynamic state of the system is fully described by four variables: time τ, relative displacement p and velocity y of the mass, and relative displacement of the slider top, q. However, this number was reduced by two by choosing the beginning of the progression phase as the point to be monitored. The lower and the upper bounds of the map domain were approximated. A graphical method of iteration of the two-dimensional map similar to the cobweb method, used in the one-dimensional case, was proposed.

The results of numerical iterations of this two-dimensional map show the complexity of the system with responses ranging from periodic to chaotic. In contrast to the classical Poincaré map, where the trajectory is sampled once per period of the external excitation, for our two-dimensional map the points are taken at the beginning of the progression phase. As a result, the duration and the shape of the periodic orbits are not known *a priori*. For this reason, it was understood that period-2 motion on the bifurcation diagram calculated for this map appears as period-1 motion on the bifurcation diagrams calculated for the original system.

Calculation of the duration of the *contact with progression* phase and the progression as functions of the variables of the developed 2D map, i.e., the angular displacement and the velocity of the mass, appears to be useful from the application point of view. These functions clearly show the level of progression for the given set of system parameters and might be used for the development of control strategies for vibroimpact devices.

ACKNOWLEDGMENT

This research was supported by EPSRC under Grant No. GR/R85556/01.

APPENDIX A

The solutions for each phase are given here.

For the *no contact* phase,

$$p^I(\tau) = p_0 + y_0(\tau-\tau_0) + \frac{b}{2}(\tau-\tau_0)^2 - \frac{a}{\omega^2}[\cos(\omega\tau+\varphi) - \cos(\omega\tau_0+\varphi) + \omega(\tau-\tau_0)\sin(\omega\tau_0+\varphi)],$$

$$y^I(\tau) = y_0 + b(\tau-\tau_0) + \frac{a}{\omega}[\sin(\omega\tau+\varphi) - \sin(\omega\tau_0+\varphi)],$$

$$q^I(\tau) = q_0\exp\left(-\frac{\tau-\tau_0}{2\xi}\right). \tag{A1}$$

For the *contact without progression* phase,

$$p^{II}(\tau) = b + g + \exp[-\xi(\tau-\tau_0)]\sqrt{C_1^2+C_2^2}\sin[\sqrt{1-\xi^2}(\tau-\tau_0) + \beta] + \frac{a}{\sqrt{(1-\omega^2)^2+4\xi^2\omega^2}}\sin(\omega\tau+\varphi+\alpha),$$

$$y^{II}(\tau) = \exp[-\xi(\tau-\tau_0)]\sqrt{C_1^2+C_2^2}\sin[\sqrt{1-\xi^2}(\tau-\tau_0)+\delta] + \frac{a\omega}{\sqrt{(1-\omega^2)^2+4\xi^2\omega^2}}\cos(\omega\tau+\varphi+\alpha),$$

$$q^{II}(\tau) = b + \exp[-\xi(\tau-\tau_0)]\sqrt{C_1^2+C_2^2}\sin[\sqrt{1-\xi^2}(\tau-\tau_0)+\beta] + \frac{a}{\sqrt{(1-\omega^2)^2+4\xi^2\omega^2}}\sin(\omega\tau+\varphi+\alpha), \tag{A2}$$

where

$$C_1 = p_0 - b - g - \frac{a}{\sqrt{(1-\omega^2)^2+4\xi^2\omega^2}}\sin(\omega\tau_0+\varphi+\alpha), \tag{A3}$$

$$C_2 = \frac{1}{\sqrt{1-\xi^2}}\left\{y_0 + \xi(p_0-b-g) - \frac{a\sqrt{\xi^2+\omega^2}}{\sqrt{(1-\omega^2)^2+4\xi^2\omega^2}}\sin(\omega\tau_0+\varphi+\alpha+\gamma)\right\},$$

$$\alpha = \arctan\left(\frac{1-\omega^2}{2\xi\omega}\right),$$

$$\beta = \arctan\left(\frac{C_1}{C_2}\right),$$

$$\gamma = \arctan\left(\frac{\omega}{\xi}\right),$$

$$\delta = \arctan\left(\frac{-\xi C_1 + \sqrt{1-\xi^2}C_2}{-\sqrt{1-\xi^2}C_1 - \xi C_2}\right). \tag{A4}$$

For the *contact with progression* phase,

$$p^{III}(\tau) = g + 1 + (p_0 - g - d)\exp\left(-\frac{\tau - \tau_0}{2\xi}\right),$$

$$y^{III}(\tau) = y_0 + (b - d)(\tau - \tau_0) + \frac{a}{\omega}[\sin(\omega\tau + \varphi) - \sin(\omega\tau_0 + \varphi)],$$

$$q^{III}(\tau) = (q_0 - d)\exp\left(-\frac{\tau - \tau_0}{2\xi}\right) + 1. \tag{A5}$$

APPENDIX B

The method of obtaining the estimation (16) is outlined below. As the solutions (A5) for the *contact with progression* phase contain exponential functions rapidly converging to zero, for any initial conditions the relative displacement of mass and slider are $\approx 1+g$ and ≈ 1, respectively, the velocity of the mass is ≈ 0, and the only arbitrariness left is in the phase shift at the end of this phase. Thus the initial conditions for the next phase, *contact without progression*, are known apart from the phase shift, and the values of both displacements and velocity during this new phase can be estimated from Eq. (A2):

$$b + g - K_1 - K_2 < p < b + g + K_1 + K_2,$$

$$-\omega K_1 - K_2 < y < \omega K_1 + K_2,$$

$$b - K_1 - K_2 < q < b + K_1 + K_2,$$

$$0 < \psi < 2\pi, \tag{B1}$$

where K_1 and K_2 are given by Eqs. (17) and (18). The inequalities (B1) determine all possible initial conditions for the next phase, *no contact*. It should be noted that the precisely determined initial conditions may belong to narrower regions, but they are certainly included by (B1). Let us find now the maximum velocity at the end of the *no contact* phase. Using the solutions (A1) one can obtain

$$y < \frac{2a}{\omega} + b\Delta\tau, \tag{B2}$$

where $\Delta\tau$ is the duration of the *no contact* phase. $\Delta\tau$ is the solution of the equation $p(\Delta\tau)=g$, where $p(\tau)$ is calculated from Eq. (A1):

$$p_0 + y_0(\Delta\tau) + \frac{b}{2}(\Delta\tau)^2 - \frac{a}{\omega^2}\{\cos[\omega(\Delta\tau) + \psi_0] - \cos(\psi_0) + \omega(\Delta\tau)\sin(\psi_0)\} = g. \tag{B3}$$

p_0, y_0, and ψ_0 are the initial conditions for the *no contact* phase which belong to the regions (B1). Now, according to Eq. (B2), in order to determine the maximum velocity, the longest possible duration $\Delta\tau$ of the *no contact* phase should be found.

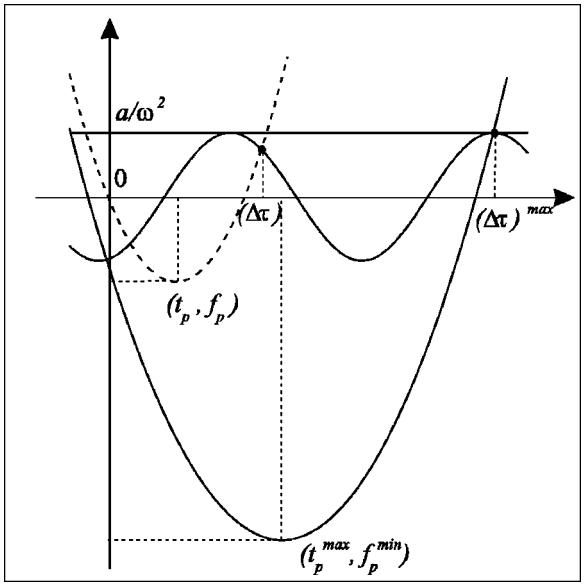

FIG. 10. Schematic to estimate $(\Delta\tau)_{max}$.

Equation (B3) can be rewritten as

$$\frac{b}{2}(\Delta\tau)^2 + \left(y_0 - \frac{a}{\omega}\sin(\psi_0)\right)\Delta\tau + p_0 - g + \frac{a}{\omega^2}\cos(\psi_0) = \frac{a}{\omega^2}\cos(\omega\Delta\tau + \psi_0). \tag{B4}$$

As can be seen from Eq. (B4), the solution $\Delta\tau$ is a point of intersection of the parabola given in the left-hand side and the cosine function given in the right-hand side of Eq. (B4), which is schematically shown in Fig. 10. As the coefficient attached to $(\Delta\tau)^2$ is constant, the point of intersection of these two curves depends on the position of the parabola minimum and the phase of the cosine function. The values of p_0, y_0, and ψ_0 define the minimum:

$$t_p = -\frac{y_0}{b} + \frac{a}{\omega b}\sin(\psi_0), \quad f_p = p_0 - g + \frac{a}{\omega^2}\cos(\psi_0) - \frac{[y_0 - a\,\sin(\psi_0)/\omega]^2}{2b}. \tag{B5}$$

$\Delta\tau$ will reach its maximum if the right branch of the parabola intersects the cosine function (see Fig. 10). This maximum will occur for the cosine function having a local maximum, i.e.,

$$\frac{b}{2}[(\Delta\tau) - t_p]^2 + f_p = \frac{a}{\omega^2}.$$

Thus

$$(\Delta\tau)^{max} = t_p^{max} + \sqrt{\frac{2}{b}\left(\frac{a}{\omega^2} - f_p^{min}\right)}.$$

It is possible to estimate t_p^{max} and f_p^{min} using the regions (B1) and expressions (B5):

$$t_p^{max} \leqslant \frac{\omega K_1 + K_2}{b} + \frac{a}{\omega b},$$

$$f_p^{min} \geqslant b - K_1 - K_2 - \frac{a}{\omega^2} - \frac{(\omega K_1 + K_2 + a/\omega)^2}{2b}.$$

Thus

$$(\Delta\tau)_{max} < \frac{1}{b}\left[\frac{a}{\omega} + \omega K_1 + K_2 + \sqrt{2b\left(K_1 + K_2 - b + \frac{2a}{\omega^2}\right) + \left(\frac{a}{\omega} + \omega K_1 + K_2\right)^2}\right], \quad \text{(B6)}$$

and substituting Eq. (B6) into (B2) we obtain an estimation of maximum velocity at the end of the *no contact* phase $y < K_3$, where K_3 is given by Eq. (19).

The next phase is again the *contact without progression* phase, and the maximum velocity for this phase gives the upper estimation for the initial velocity of the next *contact with progression* phase. Using the solution (A2), one can easily obtain

$$y < \sqrt{\tilde{C}_1^2 + \tilde{C}_2^2} + aK_1, \quad \text{(B7)}$$

where $\tilde{C}_1$ and $\tilde{C}_2$ depend on the initial conditions for this phase. At the beginning of the *contact without progression* phase, the relative displacement of the mass p is equal to g, and the velocity does not exceed the value K_3. Substituting these values as the initial conditions into Eqs. (A3) and (A4), calculating the maximum of $\sqrt{\tilde{C}_1^2 + \tilde{C}_2^2}$, and then substituting the result into Eq. (B7), we have finally arrived at the estimation given in Eq. (16):

$$y < \omega K_1 + \sqrt{(b + K_1)^2 + \frac{1}{1 - \xi^2}(K_3 - \xi b + K_1\sqrt{\xi^2 + \omega^2})^2}.$$

[1] H. Goyda and C. Teh, J. Pressure Vessel Technol. **111**, 394 (1989).
[2] M. Davies and B. Balachandran, Nonlinear Dyn. **22**, 375 (2000).
[3] M. Wiercigroch, R. D. Neilson, and M. A. Player, Phys. Lett. A **259**, 91 (1999).
[4] K.-C. Woo, A. A. Rodger, R. D. Neilson, and M. Wiercigroch, Chaos, Solitons Fractals **11**, 2515 (2000).
[5] A. E. Kobrinskii, *Dynamics of Mechanisms with Elastic Connections and Impact Systems* (ILIFFE Books, London, 1969).
[6] F. Peterka, Acta Tech. CSAV **4**, 462 (1974).
[7] J. M. T. Thompson and R. Ghaffari, Phys. Rev. A **27**, 1741 (1983).
[8] S. W. Shaw and P. J. Holmes, J. Sound Vib. **90**, 129 (1983).
[9] S. Foale and S. R. Bishop, Philos. Trans. R. Soc. London, Ser. A **338**, 547 (1992).
[10] W. Chin, E. Ott, H. E. Nusse, and C. Grebogi, Phys. Rev. E **50**, 4427 (1994).
[11] S. Banerjee and C. Grebogi, Phys. Rev. E **59**, 4052 (1999).
[12] A. M. Krivtsov and M. Wiercigroch, Meccanica **34**, 425 (1999).
[13] A. M. Krivtsov and M. Wiercigroch, Chaos, Solitons Fractals **11**, 2479 (2000).
[14] E. Pavlovskaia, M. Wiercigroch, and C. Grebogi, Phys. Rev. E **64**, 056224 (2001).
[15] E. E. Pavlovskaia and M. Wiercigroch, J. Sound Vib. **267**, 893 (2003).
[16] E. Pavlovskaia and M. Wiercigroch, Chaos, Solitons Fractals **19**, 151 (2003).
[17] M. Oestreich, N. Hinrichs, and K. Popp, Arch. Appl. Mech. **66**, 301 (1996).
[18] N. Hinrichs, M. Oestreich, and K. Popp, Chaos, Solitons Fractals **8**, 535 (1997).
[19] U. Galvanetto and S. R. Bishop, Comput. Methods Appl. Mech. Eng. **163**, 373 (1998).
[20] U. Galvanetto, Comput. Methods Appl. Mech. Eng. **178**, 291 (1999).
[21] U. Galvanetto, Comput. Phys. Commun. **131**, 1 (2000).
[22] U. Galvanetto, Comput. Methods Appl. Mech. Eng. **190**, 6075 (2001).
[23] A. B. Nordmark, J. Sound Vib. **145**, 279 (1991).
[24] M. di Bernardo, M. I. Feigin, S. J. Hogan, and M. E. Holmer, Chaos, Solitons Fractals **10**, 1881 (1999).
[25] C. Budd and F. Dux, Philos. Trans. R. Soc. London, Ser. A **347**, 365 (1994).
[26] M. di Bernardo, P. Kowalczyk, and A. Nordmark, Physica D **170**, 175 (2002).
[27] H. Dankowicz and A. Nordmark, Physica D **136**, 280 (2000).
[28] M. di Bernardo, C. J. Budd, and A. R. Champneys, Physica D **160**, 222 (2001).
[29] H. E. Nusse and J. A. Yorke, Physica D **57**, 39 (1992).
[30] M. Wiercigroch, J. Sound Vib. **175**, 700 (1994).
[31] U. Galvanetto and S. R. Bishop, Int. J. Mech. Sci. **36**, 683 (1994).